

TUTORIAL OPEN ACCESS

# SpatialCNS-PBPK: An R/Shiny Web-Based Application for Physiologically Based Pharmacokinetic Modeling of Spatial Pharmacokinetics in the Human Central Nervous System and Brain Tumors

Charuka D. Wickramasinghe  | Seongho Kim | Jing Li 

Karmanos Cancer Institute, Wayne State University School of Medicine, Detroit, Michigan, USA

**Correspondence:** Jing Li ([lijing@wayne.edu](mailto:lijing@wayne.edu))**Received:** 27 November 2024 | **Revised:** 21 February 2025 | **Accepted:** 18 March 2025**Funding:** This study is supported by the National Cancer Institute of the National Institutes of Health (NIH) R01CA255124 (JL) and NIH Cancer Center Support Grant P30CA022453 (Karmanos Cancer Institute Pharmacology and Metabolomics Core, Biostatistics and Bioinformatics Core).**Keywords:** brain cancer drug development | central nervous system pharmacokinetics | physiologically based pharmacokinetic (PBPK) model | R/shiny interface | spatial pharmacokinetics

## ABSTRACT

Quantitative understanding of drug penetration and exposure in the human central nervous system (CNS) and brain tumors is essential for the rational development of new drugs and optimal use of existing drugs for brain cancer. To address this need, we developed and validated a novel 9-compartment permeability-limited CNS (9-CNS) physiologically based pharmacokinetic (PBPK) model, enabling mechanistic and quantitative prediction of spatial pharmacokinetics for systemically administered small-molecule drugs across different regions of the human brain, cerebrospinal fluid, and brain tumors. To make the 9-CNS model accessible to a broad range of users, we developed the SpatialCNS-PBPK app, a user-friendly, web-based R/Shiny platform built with R and Shiny programming. The app provides key functionalities for model simulation, sensitivity analysis, and pharmacokinetic parameter calculation. This tutorial introduces the development and evaluation of the SpatialCNS-PBPK app, highlights its key features and functions, and provides a step-by-step user guide for practical applications. By enhancing our ability to predict the spatial pharmacokinetics of anticancer drugs in the human CNS and brain tumors, the SpatialCNS-PBPK app serves as an invaluable computational tool and data-driven approach for advancing drug development and optimizing treatment strategies for more effective treatment of brain cancer.

## 1 | Introduction

Drug delivery to the brain is restrained by the blood–brain barrier (BBB), a physical and biochemical barrier separating the brain parenchyma from the circulatory system [1]. In brain tumors, the integrity and function of the BBB are disrupted to varying extents, leading to large intra- and inter-individual variability (heterogeneity) in drug penetration, which in turn impacts clinical outcome [2–4]. Quantitative knowledge of heterogeneous

drug penetration and exposure in the human central nervous system (CNS) and brain tumors is critical to the rational development of new drugs and optimal use of current drugs for brain cancer. However, the pharmacokinetics of many new and existing anticancer drugs in the human CNS and brain tumors remain poorly characterized due to challenges in sampling and limitations in current imaging and analytical technologies. Physiologically based pharmacokinetic (PBPK) modeling offers an innovative computational approach for mechanistically and

This is an open access article under the terms of the [Creative Commons Attribution-NonCommercial-NoDerivs](https://creativecommons.org/licenses/by-nc-nd/4.0/) License, which permits use and distribution in any medium, provided the original work is properly cited, the use is non-commercial and no modifications or adaptations are made.

© 2025 The Author(s). *CPT: Pharmacometrics & Systems Pharmacology* published by Wiley Periodicals LLC on behalf of American Society for Clinical Pharmacology and Therapeutics.

quantitatively predicting CNS pharmacokinetics. By incorporating drug-specific and biological system-specific parameters into a pharmacokinetic model, the PBPK model enables the prediction of in vivo kinetic processes through mechanistic scaling of in vitro data (e.g., in vitro cellular permeability and transporter kinetic data) [5, 6].

We have developed and rigorously validated a novel 9-compartment, permeability-limited CNS (9-CNS) PBPK model to predict spatial pharmacokinetics of systemically administered small-molecule drugs in the human CNS and brain tumors [7]. The 9-CNS model was designed based on the general anatomical structure and pathophysiological heterogeneity of the human CNS and brain tumor [7]. The model consists of nine compartments including two distinct brain parenchyma compartments (representing brain tissue adjacent to the cerebrospinal fluid [CSF] tract and deep brain parenchymal region located > 2 mm from the CSF tract), three CSF compartments (ventricular CSF, cranial and spinal subarachnoid CSF), and three tumor compartments (tumor rim, bulk tumor, and tumor core) (Figure S1) [7]. Drug penetration into and distribution within the nine CNS compartments is driven by the system (plasma) drug concentration-time profile (serving as the input function) and regulated by multiple dynamic, interactive processes. Drug transfer and fluid flow between compartments are described by a system of linear nonhomogeneous ordinary differential equations incorporating both drug-specific and system-specific parameters. Compared to the existing 4-compartment CNS (4-CNS) PBPK model (Figure S2) implemented in Simcyp Simulator (Certara Inc.), which treats the brain as a homogeneous compartment [8], the 9-CNS model accounts for regional pathophysiological heterogeneity in the human CNS and brain tumors, thereby providing a mechanism-based computational tool for the prediction of spatiotemporal drug penetration and exposure in the CNS and brain tumors.

The R/Shiny interface enables the development of web applications with both front-end (visual design and interactivity) and back-end (computations and database management) capabilities. This allows users to leverage R's extensive library of packages for data science, statistical analyses, and modeling. While several Shiny-based tools have been developed for pharmacokinetic/pharmacodynamic (PK/PD) analysis [9–12], none have been specifically designed for PBPK modeling of spatial pharmacokinetics in the human CNS.

To make the 9-CNS PBPK model accessible to a broad range of users, we developed a user-friendly, web-based R/Shiny platform, named SpatialCNS-PBPK. The SpatialCNS-PBPK app (*patent application #, US63/684,242*) is available at: [https://pbpklab.shinyapps.io/SpatialCNS\\_PBPK\\_V1/](https://pbpklab.shinyapps.io/SpatialCNS_PBPK_V1/). The app is programmed in R using Shiny as the web framework and integrates key R packages (e.g., tidyverse, deSolve, ggplot2, and dplyr) to enable efficient data handling, differential equation solving, and interactive visualization [13–17]. This tutorial presents the development and validation of the SpatialCNS-PBPK app, highlights its key features and functionalities, and provides a step-by-step user guide for practical applications in predicting spatial pharmacokinetics in the human CNS and brain tumors.

## 2 | 9-CNS PBPK Model

### 2.1 | Model Structure and Hypotheses

The 9-CNS PBPK model (Figure S1) comprises nine compartments, including a brain blood compartment, two brain parenchyma compartments (representing brain tissue adjacent to CSF and a deep brain region > 2 mm from the CSF tract), three CSF compartments (ventricular CSF, cranial subarachnoid space, and spinal subarachnoid space), and three tumor compartments (infiltrative tumor rim, bulk tumor, and tumor core). In the 9-CNS model, each brain or tumor compartment is treated as homogeneous, with the unbound drug rapidly distributing between the interstitial and intracellular spaces to reach equilibrium and exert pharmacological effects. Hence, the model-predicted total and unbound drug concentrations (linked by unbound fraction in tissue:  $\text{unbound concentration} = \text{total concentration} \times \text{unbound fraction}$ ) can be readily validated by comparing the predicted values with measured concentrations from brain/tumor tissue homogenates (which are commonly available from pre-clinical or clinical studies) [7].

Following systemic drug administration, drug distribution into and within the nine CNS compartments is driven by drug plasma concentration-time profile (serving as the input function in the 9-CNS model) and governed by CNS physiological processes, as detailed previously [7]. Briefly, drug transport across the BBB, blood-brain tumor barrier (BBTB), and blood-CSF barrier is governed by passive permeability and transporter-mediated active transport [18–20]. Once in the CSF, drug flows through the ventricular system to the cranial and spinal subarachnoid spaces and is subsequently drained into the systemic circulation [21–23]. Drug distribution from the ventricular and subarachnoid CSF across the ependymal lining into the adjacent brain tissue primarily occurs via simple diffusion [23]. Drug may distribute between the CSF tract and deep brain parenchyma or tumors through paravascular convective bulk flow, commonly referred to as the glymphatic system [24].

The 9-CNS model incorporates regional pathophysiological heterogeneity in the normal brain parenchyma and tumor compartments, as detailed previously [7]. The model considers variability in the BBB integrity and transporter function across the normal brain and brain tumors. It assumes that the BBB maintains intact tight junctions in the brain parenchyma and infiltrative tumor rim, while tight junctions are progressively disrupted in the bulk tumor and tumor core compartments. This disruption could lead to a 2- to 50-fold increase in passive permeability at the BBTB in these compartments. Transporter-mediated active efflux clearance at the BBB varies between the brain parenchyma and tumor compartments, reflecting the heterogeneity of transporter expression or function [25]. In addition, the model accounts for regional differences in interstitial pH across the normal brain and tumor compartments, which impacts drug ionization and permeability. The normal brain parenchyma has an interstitial pH of 7.2, while tumor regions exhibit progressively more acidic conditions (e.g., 6.8 in the tumor rim, 6.5 in bulk tumor, and 6.2 in the tumor core) [26–28]. Furthermore, the 9-CNS model considers pathophysiological changes caused by tumor edema, which affects fluid dynamics in the brain and tumor

compartments. For instance, the paravascular bulk flow rate is assumed to be doubled in the tumor rim due to edema-induced expansion of the tumor's extracellular water volume, whereas it is reduced in the bulk tumor and tumor core due to increased interstitial pressure. Additionally, considering the potential for different tissue compositions and plasma protein extravasation in tumor edema, the model incorporates changes in drug binding across the brain parenchyma and various tumor compartments.

## 2.2 | Model Equations

Drug distribution and fluid flow into and out of individual compartments of the 9-CNS PBPK model are described by differential equations that contain system-specific and drug-specific parameters, as presented in Supporting Information. The system- and drug-specific parameters are defined in Tables 1 and 2.

## 2.3 | Methods for Solving Differential Equations

The rates of change in drug concentrations in individual compartments of the 9-CNS PBPK model are described by a system of non-homogeneous linear parametric ordinary differential equations (ODEs). Various numerical methods exist for solving systems of differential equations, such as Euler's method, Runge-Kutta methods, and Adam's method. Each method carries its own strengths and weaknesses. In our study, we employed the Livermore Solver for Ordinary Differential Equations with Automatic method (LSODA) available through the deSolve package in R to efficiently solve the differential equations of the 9-CNS model [29]. LSODA automatically selects between non-stiff and stiff methods by dynamically monitoring data, and thus, users do not need to determine whether the system of differential equations is stiff or not. For solving non-stiff systems of ordinary differential equations, LSODA offers the implicit Adams method [30]. For solving stiff systems of differential equations, LSODA uses the backward differentiation formula (BDF) method, which is commonly used for solving such problems [31–33]. However, it always starts with the non-stiff method. The discrete drug plasma concentration-time profile is converted into a continuous profile (used as the input function of the model) via linear interpolation as this is required by the ODE function and passed to the ODE function as an additional argument. Finally, the ODE function within the deSolve package retrieves state variable values (i.e., drug concentrations) from the 9-CNS model at specified times (i.e., sampling times).

## 3 | Evaluation of the SPATIALCNS PBPK App

A 4-compartment permeability-limited CNS (4-CNS) PBPK model is implemented in the Simcyp Simulator v18. The model structure, differential equations, and system-specific parameters for the 4-CNS model were published [18]. To evaluate the SpatialCNS-PBPK app, we packaged the 4-CNS PBPK model into the SpatialCNS-PBPK app using the same methodology as that for the 9-CNS model, and then we compared the 4-CNS

model simulation results from the Simcyp Simulator v18 and SpatialCNS-PBPK app.

Ribociclib was used as the model drug for model evaluation. First, we performed simulations with the Simcyp 4-CNS model to predict ribociclib concentration—time profiles in the plasma, brain mass, cranial, and spinal CSF compartments in 100 Simcyp virtual cancer patients (i.e., 10 trials with 10 cancer patients in each trial) following oral administration of a single dose (600 mg). The drug- and system-specific parameters for the Simcyp whole-body-4-CNS PBPK model of ribociclib were published previously by us [20]. Then, using the Simcyp 4-CNS model-simulated ribociclib plasma concentration—time profiles from 100 individuals as the input function, we performed simulations with the app 4-CNS model to predict the drug concentration—time profiles in the brain mass, cranial, and spinal CSF compartments for the same 100 individuals, where the system- and drug-specific parameters were the same as those used in the Simcyp 4-CNS model simulations [20]. The input file template for the app 4-CNS model is provided in Table S1.

Based on the 4-CNS model-simulated ribociclib concentration-time profile by the Simcyp Simulator and SpatialCNS-PBPK app from the same 100 individuals, the mean and inter-individual variability (represented by 5th and 95th percentiles) of the concentration profiles in individual four CNS compartments were generated. As shown in Figure S3, the mean, 5th and 95th percentiles of ribociclib concentration profiles in individual CNS compartments simulated from the SpatialCNS-PBPK app were well aligned with those simulated from the Simcyp Simulator. Further correlation analysis indicated a Pearson's correlation coefficient (R) of approximately 1 between the Simcyp and SpatialCNS-PBPK app simulated mean concentrations in individual CNS compartments. Collectively, these data suggested that the methodology used in the SpatialCNS PBPK app, including the method for solving differential equations, was validated by the Simcyp Simulator.

## 4 | SPATIALCNS-PBPK App Functions and User Guide

The SpatialCNS-PBPK app is a graphical user interface that consists of two modules: model simulation and sensitivity analysis, as shown in Figure 1. After an input file is uploaded, users can perform model simulations to predict drug concentration-time profiles in individual CNS compartments. In addition, users can perform sensitivity analysis to examine the impact of a particular system- or drug-specific parameter on the drug concentration-time profiles in individual compartments. The app provides real-time updates of outputs in response to input modifications and allows users to visualize the simulated plots and data tables. In addition, the output results including simulated drug concentration-time plots and data tables as well as calculated pharmacokinetic parameters can be downloaded. A step-by-step user guide for preparing the input file and performing model simulation and sensitivity analysis is provided as follows, using abemaciclib as the model drug.

**TABLE 1** | System-specific parameters for the 9-CNS PBPK model.

Parameters	Descriptions	Values	References or Assumptions
$V_{bb}$ (L)	Volume of brain blood	0.0630	5% of brain volume (1260 cm <sup>3</sup> in men and 1130 cm <sup>3</sup> in women) (ref 22)
$V_{bm1}$ (L)	Volume of adjacent brain tissue	0.1200	Assuming 10% of brain volume (average brain volume, 1.2 L)
$V_{bm2}$ (L)	Volume of deep brain parenchyma	1.0800	Assuming 90% of brain volume (average brain volume, 1.2 L)
$V_{T1}$ (L)	Volume of infiltrative tumor region	0.0700	Assuming non-enhancing tumor is 2-fold of enhancing tumor volume
$V_{T2}$ (L)	Volume of bulky tumor region	0.0350	Assuming enhancing tumor is 35 mL
$V_{T3}$ (L)	Volume of tumor core	0.0035	Assuming tumor core is 10% of enhancing tumor volume
$V_{vcsf}$ (L)	Volume of ventricular CSF	0.0251	16.7% of total CSF (0.15 L) (ref 22)
$V_{ccsf}$ (L)	Volume of cranial subarachnoid CSF	0.0450	30% of total CSF (0.15 L) (ref 22)
$V_{scsf}$ (L)	Volume of spinal subarachnoid CSF	0.0800	SCSF is 80 mL (ref 36)
$Q_{brain}$ (L/h)	Cerebral blood flow	39.0000	600–700 mL/min or 15% of the cardiac output (ref 22, 36)
$Q_{csink}$ (L/h)	Absorption rate of cranial CSF into blood circulation through arachnoid villi	0.0130	62% of CSF production rate (0.021 L/h) (ref 38)
$Q_{ssink}$ (L/h)	Absorption rate of spinal CSF into blood circulation through arachnoid villi	0.0080	38% of CSF production rate (0.021 L/h) (ref 38)
$Q_{gly,ccsf}$ (L/h)	Absorption rate of cranial CSF via olfactory mucosa and cranial nerve sheaths	0.0065	50% of $Q_{csink}$
$Q_{gly,scsf}$ (L/h)	Absorption rate of spinal CSF via spinal nerve sheaths	0.0040	50% of $Q_{ssink}$
$Q_{sin1}$ (L/h)	CSF flow rate from the ventricle to cranial subarachnoid space	0.0126	60% of CSF production rate (0.021 L/h) (ref 38)
$Q_{sin1r}$ (L/h)	CSF back flow rate from the cranial subarachnoid space to ventricle	0.0013	Assuming 10% of $Q_{sin1}$
$Q_{sin2}$ (L/h)	CSF flow rate from the ventricle to spinal subarachnoid space	0.0084	40% of CSF production rate (0.021 L/h) (ref 38)
$Q_{sin2r}$ (L/h)	CSF back flow rate from the spinal subarachnoid space to ventricle	0.0008	Assuming 10% of $Q_{sin2}$
$Q_{sout}$ (L/h)	CSF flow rate from the spinal subarachnoid space to cranial subarachnoid	0.0004	Assuming $Q_{sout} = Q_{csink} - Q_{sin1}$ to maintain fluid balance
$Q_{soutr}$ (L/h)	CSF flow rate from the cranial subarachnoid space to spinal subarachnoid	0.0000	Assuming 10% of $Q_{sout}$
$Q_{bulk,CB1}$ (L/h)	Paravascular bulk flow rate from the cranial subarachnoid CSF to brain parenchyma 1	0.0013	Average bulk flow rate is 0.15 ul/min/g in human brain, bm1 is 10% of whole brain weight (140 g)
$Q_{bulk,B1C}$ (L/h)	Paravascular bulk flow rate from brain parenchyma 1 to cranial subarachnoid CSF	0.0016	Assuming 1.25-fold of $Q_{bulk,CB1}$
$Q_{bulk,VB1}$ (L/h)	Paravascular bulk flow rate from the ventricular CSF to brain parenchyma 1	0.0001	Assuming 10% of $Q_{bulk,CB1}$
$Q_{bulk,B1V}$ (L/h)	Paravascular bulk flow rate from brain parenchyma 1 to ventricular CSF	0.0002	Assuming 1.25-fold of $Q_{bulk,VB1}$

(Continues)

**TABLE 1** | (Continued)

Parameters	Descriptions	Values	References or Assumptions
$Q_{\text{bulk,CB2}}$ (L/h)	Paravascular bulk flow rate from cranial subarachnoid CSF to brain parenchyma 2	0.0113	Average bulk flow rate is 0.15 ul/min/g in human brain, bm2 is 90% of whole brain weight (1260g) (ref 37)
$Q_{\text{bulk,B2C}}$ (L/h)	Paravascular bulk flow rate from brain parenchyma 2 to cranial subarachnoid CSF	0.0142	Assuming 1.25-fold of $Q_{\text{bulk,CB2}}$
$Q_{\text{bulk,CT1}}$ (L/h)	Paravascular bulk flow rate from cranial subarachnoid CSF to tumor mass 1	0.0013	Assuming bulk flow rate increased 2-fold (0.30 ul/min/g) in tumor rim (T1) due to tumor edema; assuming T1 is 70g.
$Q_{\text{bulk,T1C}}$ (L/h)	Paravascular bulk flow rate from tumor mass 1 to cranial subarachnoid CSF	0.0016	Assuming 1.25-fold of $Q_{\text{bulk,CT1}}$
$Q_{\text{bulk,CT2}}$ (L/h)	Paravascular bulk flow rate from cranial subarachnoid CSF to tumor mass 2	0.0002	Assuming bulk flow rate decreased by 25% (0.1125 ul/min/g) in bulk tumor (T2) due to increased interstitial pressure; assuming T2 is 35g.
$Q_{\text{bulk,T2C}}$ (L/h)	Paravascular bulk flow rate from tumor mass 2 to cranial subarachnoid CSF	0.0003	Assuming 1.25-fold of $Q_{\text{bulk,CT2}}$
$Q_{\text{bulk,CT3}}$ (L/h)	Paravascular bulk flow rate from cranial subarachnoid CSF to tumor mass 3	0.0000	Assuming bulk flow rate decreased by 50% (0.075 ul/min/g) in tumor core (T3) due to increased interstitial pressure; assuming T3 weight is 20% of T1
$Q_{\text{bulk,T3C}}$ (L/h)	Paravascular bulk flow rate from tumor mass 3 to cranial subarachnoid CSF	0.0000	Assuming 1.25-fold of $Q_{\text{bulk,CT3}}$
$Q_{\text{bulk,B1B2}}$ (L/h)	Convective bulk flow rate from brain parenchyma 1 to 2	0.0005	Assuming a constant small bulk flow between two brain parenchyma compartments
$Q_{\text{bulk,B2B1}}$ (L/h)	Convective bulk flow rate from brain parenchyma 2 to 1	0.0005	Assuming a constant small bulk flow between two brain parenchyma compartments
$Q_{\text{bulk,B2T1}}$ (L/h)	Convective bulk flow rate from brain parenchyma 2 to tumor mass 1	0.0005	Assuming a constant small bulk flow between the brain and tumor rim compartments
$Q_{\text{bulk,T1B2}}$ (L/h)	Convective bulk flow rate from tumor mass 1 to brain parenchyma 2	0.0005	Assuming a constant small bulk flow between the brain and tumor rim compartments
$Q_{\text{bulk,T1T2}}$ (L/h)	Convective bulk flow rate from tumor mass 1 to 2	0.0002	Assuming a constant small bulk flow between tumor rim and bulk tumor
$Q_{\text{bulk,T2T1}}$ (L/h)	Convective bulk flow rate from tumor mass 2 to 1	0.0002	Assuming a constant small bulk flow between tumor rim and bulk tumor
$Q_{\text{bulk,T2T3}}$ (L/h)	Convective bulk flow rate from tumor mass 2 to 3	0.0002	Assuming a constant small bulk flow between bulk tumor and tumor core
$Q_{\text{bulk,T3T2}}$ (L/h)	Convective bulk flow rate from tumor mass 3 to 2	0.0002	Assuming a constant small bulk flow between bulk tumor and tumor core

## 4.1 | Prepare Input File

### 4.1.1 | Input File Template

An input file provides necessary information for model simulations, which includes the drug plasma-concentration time profile (as the input function of the model), system- and drug-specific parameters, and respective interindividual variabilities, as well as observed data (if available). An input file is prepared in .csv or .xlsx format. The template of the input file for the 9-CNS model is provided in Table S2, using abemaciclib as the model drug. The

input file contains a number of columns, named as Time (sampling times), Plasma (drug plasma concentrations), Parameters (system- and drug-specific parameter names), IIV (interindividual variability), and Sim (parameter values). In addition, observed data (e.g., measured drug concentrations in CSF and/or tumor) (if available) can be included in the input file (Table S1). Of note, users have the flexibility to add new columns for additional plasma time profiles (e.g., Time2 and Plasma2), parameter values (e.g., Sim2, Sim3...), and inter-individual variability (e.g., IIV2) for performing different simulations. However, the column names should follow the sequence of the current column names in the template, and

**TABLE 2** | Drug-specific parameters for the 9-CNS PBPK model.

Parameters	Description
MW (g/mol)	Molecular weight
LogP	Logarithm of the neutral species octanol-to-buffer partition ratio
PKa	Acid dissociation constants
PSB1 (L/h)	Passive permeability clearance at the BBB between brain blood and adjacent brain parenchyma
PSB2 (L/h) <sup>a</sup>	Passive permeability clearance at the BBB between brain blood and deep brain parenchyma
PST1 (L/h)	Passive permeability clearance at the BBTB between brain blood and tumor rim
PST2 (L/h)	Passive permeability clearance at the BBTB between brain blood and bulk tumor
PST3 (L/h)	Passive permeability clearance at the BBTB between brain blood and tumor core
PSV (L/h)	Passive permeability clearance at the blood-CSF barrier between the brain blood and ventricular CSF
PSC (L/h)	Passive permeability clearance at the blood-CSF barrier between the brain blood and cranial subarachnoid CSF
PSE1 (L/h)	Simple diffusion rate between cranial subarachnoid CSF and adjacent brain parenchyma
PSE2 (L/h)	Simple diffusion rate between ventricular CSF and adjacent brain parenchyma
PSB1B2 (L/h)	Simple diffusion rate between the adjacent and deep brain parenchyma
PSB2T1 (L/h)	Simple diffusion rate between the deep brain parenchyma and tumor rim
PST1T2 (L/h)	Simple diffusion rate between tumor rim and bulk tumor
PST2T3 (L/h)	Simple diffusion rate between bulk tumor and tumor core
CL <sub>eff,bbb1</sub> (L/h)	Efflux transporter-mediated efflux clearance at the BBB between the brain blood and adjacent brain parenchyma
CL <sub>up,bbb1</sub> (L/h)	Uptake transporter-mediated influx clearance at the BBB between the brain blood and adjacent brain parenchyma
CL <sub>eff,bbb2</sub> (L/h) <sup>b</sup>	Efflux transporter-mediated efflux clearance at the BBB between the brain blood and deep brain parenchyma
CL <sub>up,bbb2</sub> (L/h)	Uptake transporter-mediated influx clearance at the BBB between the brain blood and deep brain parenchyma

(Continues)

**TABLE 2** | (Continued)

Parameters	Description
CL <sub>eff,T1</sub> (L/h)	Efflux transporter-mediated efflux clearance at the BBTB between the brain blood and tumor rim
CL <sub>up,T1</sub> (L/h)	Uptake transporter-mediated influx clearance at the BBB between the brain blood and tumor rim
CL <sub>eff,T2</sub> (L/h)	Efflux transporter-mediated efflux clearance at the BBTB between the brain blood and bulk tumor
CL <sub>up,T2</sub> (L/h)	Uptake transporter-mediated influx clearance at the BBB between the brain blood and bulk tumor
CL <sub>eff,T3</sub> (L/h)	Efflux transporter-mediated efflux clearance at the BBTB between the brain blood and tumor core
CL <sub>up,T3</sub> (L/h)	Uptake transporter-mediated influx clearance at the BBB between the brain blood and tumor core
CL <sub>eff,vcsf</sub> (L/h)	Efflux transporter-mediated efflux clearance at the blood-CSF barrier between the brain blood and ventricular CSF compartments
CL <sub>up,vcsf</sub> (L/h)	Uptake transporter-mediated uptake clearance at the blood-CSF barrier between the brain blood and ventricular CSF compartments
CL <sub>eff,ccsf</sub> (L/h)	Efflux transporter-mediated efflux clearance at the blood-CSF barrier between the brain blood and cranial subarachnoid CSF
CL <sub>up,ccsf</sub> (L/h)	Uptake transporter-mediated uptake clearance at the blood-CSF barrier between the brain blood and cranial subarachnoid CSF
CL <sub>met1</sub> (L/h)	Drug metabolism clearance in the adjacent brain parenchyma
CL <sub>met2</sub> (L/h)	Drug metabolism clearance in the deep brain parenchyma
fubb	Drug unbound fraction in the brain blood
fubm1	Drug unbound fraction in the adjacent brain parenchyma
fubm2	Drug unbound fraction in the deep brain parenchyma
fuT1	Drug unbound fraction in tumor rim
fuT2	Drug unbound fraction in bulk tumor
fuT3	Drug unbound fraction in tumor core
fuvcsf	Drug unbound fraction in ventricular CSF
Fuccsf, fuscsf	Drug unbound fraction in cranial/spinal subarachnoid CSF

(Continues)

TABLE 2 | (Continued)

Parameters	Description
$\lambda_{bb}^c$	Unionization fraction in the brain blood (pH 7.4)
$\lambda_{bm1}^c$	Unionization fraction in the adjacent brain parenchyma (pH 7.2)
$\lambda_{bm2}^c$	Unionization fraction in the deep brain parenchyma (pH 7.2)
$\lambda_{T1}^c$	Unionization fraction in tumor rim (pH 6.8)
$\lambda_{T2}^c$	Unionization fraction in bulk tumor (pH 6.5)
$\lambda_{T3}^c$	Unionization fraction in tumor core (pH 6.2)
$\lambda_{vcsf}^c$	Unionization fraction in the ventricular CSF (pH 7.3)
$\lambda_{ccsf}, \lambda_{scsf}^c$	Unionization fraction in the cranial or spinal subarachnoid space CSF (pH 7.3)

<sup>a</sup> $PSB = \frac{P_{app,A-B} \times SA}{\lambda}$  (Equation 1), where  $P_{app,A-B}$  is the apparent permeability determined from MDCKII cell monolayer; SA is the human brain microvasculature surface area (mean, 20 m<sup>2</sup> [2]); and  $\lambda$  is unionization efficiency.

<sup>b</sup> $CL_{efflux,BBB} = CL_{efflux,vitro} \times RAF = CL_{efflux,vitro} \times \frac{Abundance\ in\ vivo}{Abundance\ in\ vitro} \times BMvPGB \times BW$ , where  $CL_{efflux,vitro}$  ( $\mu\text{L}/\text{min}/\text{mg}$ ) is the in vitro efflux transporter-mediated intrinsic clearance; RAF is the relative activity factor; BMvPGB is the milligrams of brain microvessels per gram brain; BW is the average human brain weight; abundance in vivo or in vitro represents the ABCB1/ABCG2 transporter protein expression level in human brain microvessels or in MDCKII-ABCB1 and -ABCG2 cells, respectively.

<sup>c</sup>Unionization fraction ( $\lambda$ ) is the ratio of unionized form to total drug (the sum of unionized and ionized forms), where the unionized-to-ionized ratio is calculated based on Henderson-Hasselbalch equation:  $\text{Log}_{10} \frac{\text{base (or unionized)}}{\text{acid (ionized)}} = \text{pH} - \text{PK}$ .

in addition, the same order of parameter names should be kept as shown in the template (Table S2).

#### 4.1.2 | Drug Plasma Concentration-Time Profile

The drug plasma concentration-time profile is used as the input function for the 9-CNS model simulations. Users need to provide this information in the columns named “Time” and “Plasma” in the input file. Drug plasma concentration-time profiles can be obtained from individual patients or a patient population. As described previously, we performed population plasma pharmacokinetic analysis to characterize the population mean and inter-individual variability (expressed as the 5th and 95th percentiles) of the plasma concentration-time profiles for the model drugs, which were subsequently applied as the input functions for the 9-CNS model simulations [7]. As an example, the input file template includes the population mean plasma concentration-time profile of abemaciclib determined from glioblastoma patients [7]. In addition to using the population mean plasma concentration-time profile as the input function to predict CNS pharmacokinetics in the “average” patient population, the observed plasma concentration-time profile in an individual patient can be used as the input function to predict CNS pharmacokinetics in that particular patient. Of note, observed drug plasma concentration data with either intensive or sparse sampling time can be used as the input function because the app internally converts the discrete drug plasma concentration-time profile to a continuous profile via linear interpolation.

#### 4.1.3 | System- and Drug-Specific Parameters

Users need to provide system- and drug-specific parameters in the column “Sim” in the input file (Table S2). The typical or reference values of the system-specific parameters for the 9-CNS model (as presented in Table 1 and input file template) were determined or assumed based on literature data [22, 34–37] and further validated by us using 6 different drugs [7]. Users can use these typical values as the starting point for simulations and modify them if needed.

The drug-specific parameters are defined in Table 2. As an example, the input file template (Table S2) includes the drug-specific parameter values for abemaciclib, as published previously by us [7]. Users need to provide drug-specific parameter values for their model drugs. The methods for determination of drug-specific parameters were described briefly below, and details can be found in published papers [7, 19, 20].

Mechanistic in vitro-in vivo extrapolation (IVIVE) strategy is used to predict in vivo passive clearance and transporter-mediated active efflux clearance at the BBB. Specifically, in vivo passive clearance at the BBB or BBTB, parameterized as the passive permeability-surface area product (PSB), can be estimated by scaling of the apical-to-basolateral apparent permeability ( $P_{app,A-B}$ ) determined from in vitro epithelial cell model to the human brain/tumor microvasculature surface area (SA) using the equation:  $PSB = \frac{P_{app,A-B} \times SA}{\lambda}$ , where  $P_{app,A-B}$  is corrected by the unionization fraction ( $\lambda$ ) of a drug because passive permeability allows only unbound and unionized drug to pass through [18, 38]. The unionization efficiency ( $\lambda$ ) is calculated using the Henderson-Hasselbalch equation:  $\text{Log}_{10} \frac{\text{base (or unionized)}}{\text{acid (ionized)}} = \text{pH} - \text{PK}$  [19, 20]. The active efflux clearance at the BBB ( $CL_{efflux,BBB}$ ) can be estimated based on the intrinsic efflux clearance ( $CL_{efflux,vitro}$ ) determined from in vitro transporter system using the equation:  $CL_{efflux,BBB} = CL_{efflux,vitro} \times RAF \times BMvPGB \times BW$ , where  $CL_{efflux,vitro}$  is the in vitro efflux transporter-mediated intrinsic clearance determined from MDCKII cells with stable expression of an efflux transporter (e.g., ABCB1 or ABCG2), RAF is the in vivo-in vitro relative activity factor of the transporter, BMvPGB is the milligrams of brain microvessels per gram brain/tumor, BW is the brain/tumor weight. Drug unbound fraction ( $F_u$ ) in human plasma and brain/tumor can be experimentally determined from the plasma and brain tumor samples [39–46].

## 4.2 | Perform Model Simulations

### 4.2.1 | Upload Input File and Select Inputs

To perform model simulations, users need to upload the input file from the user's local directory and select the inputs for sampling time (e.g., Time1), plasma concentration (e.g., Plasma1), model parameters (e.g., Sim1), IIV (e.g., IIV1), group size (i.e., number of subjects), and time range for the calculation of PK parameters (i.e.,  $C_{max}$ ,  $T_{max}$ , and AUC), as illustrated in the left panel of the app (Figure 1). The input values are read by the app from the input file and submitted for model simulation. Once the simulation is completed, users can view and download simulated concentration-time profiles, data tables, and PK parameters (calculated based on simulated data), as described below.

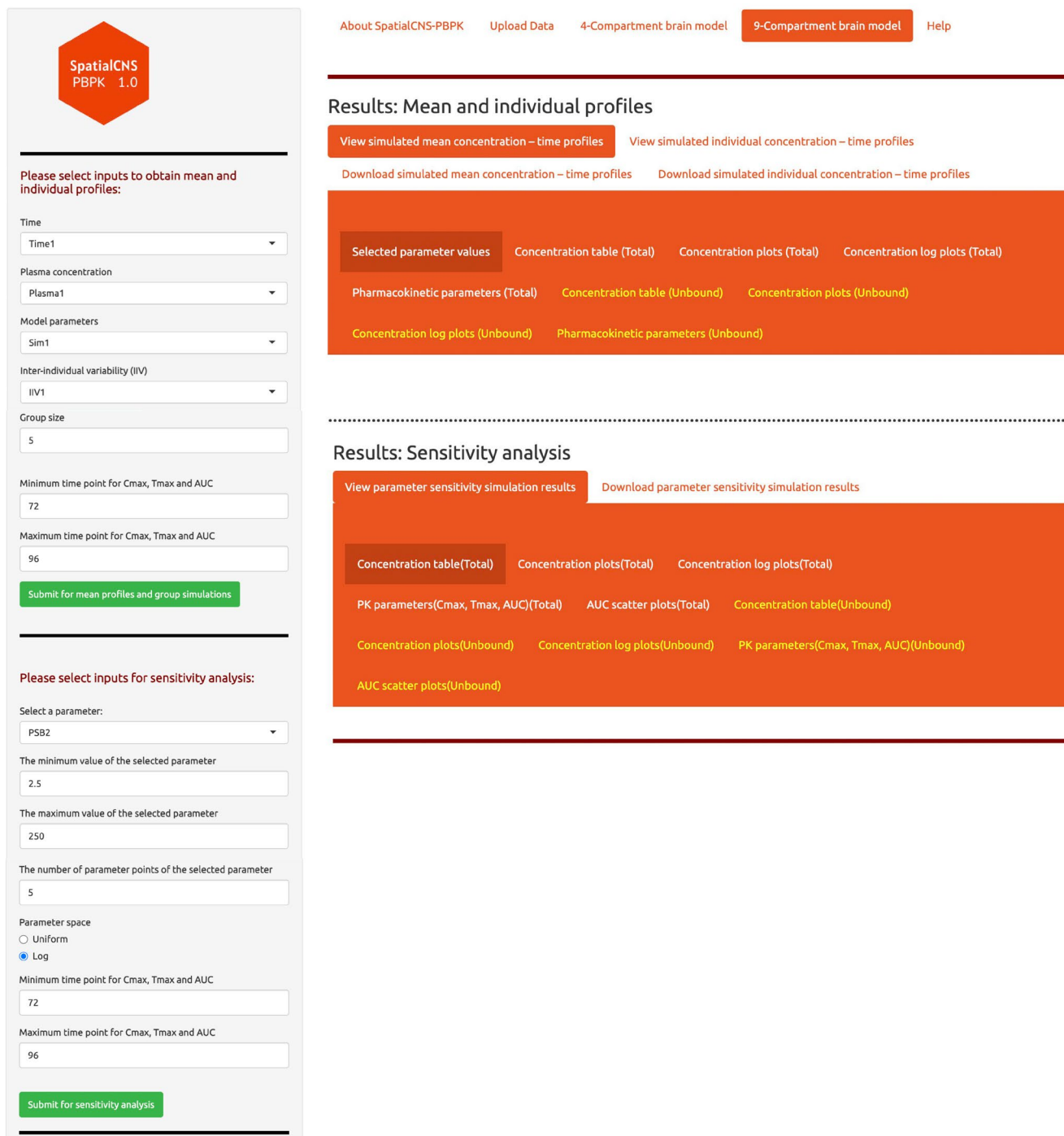


**FIGURE 1** | A screenshot illustrating the graphical user interface of the SpatialCNS-PBPK application, which consists of two modules: Model simulation and sensitivity analysis. The app provides real-time updates of outputs in response to input modifications (in the left panel) and allows users to view or download the plots and data tables from model simulation and sensitivity analysis (in the right panel).

#### 4.2.2 | View and Download Simulated Mean Concentration-Time Profiles, Concentration Data Tables, and PK Parameters

Based on the mean model parameter values provided in the input “Sim1”, the mean drug concentration-time profiles in individual CNS compartments are simulated. As illustrated in Figure 2, users can click “Simulated mean concentration-time

profile” tab to view the simulated data tables and profile plots (in either normal scale or normal logarithmic scale) for total or unbound drug; in addition, users can download data tables as .csv files and plots as .pdf files. Of note, if observed data are provided in the input file, observed data will be overlaid with the simulated profiles in the plots, thus allowing a direct visualization of how well the model predicts the observed data. As illustrated in Figure 2, observed total drug concentrations

## Results: Mean and individual profiles

[View simulated mean concentration – time profiles](#)

[View simulated individual concentration – time profiles](#)

[Download simulated mean concentration – time profiles](#)

[Download simulated individual concentration – time profiles](#)

[Selected parameter values](#)

[Concentration table \(Total\)](#)

[Concentration plots \(Total\)](#)

[Concentration log plots \(Total\)](#)

[Pharmacokinetic parameters \(Total\)](#)

[Concentration table \(Unbound\)](#)

[Concentration plots \(Unbound\)](#)

[Concentration log plots \(Unbound\)](#)

[Pharmacokinetic parameters \(Unbound\)](#)

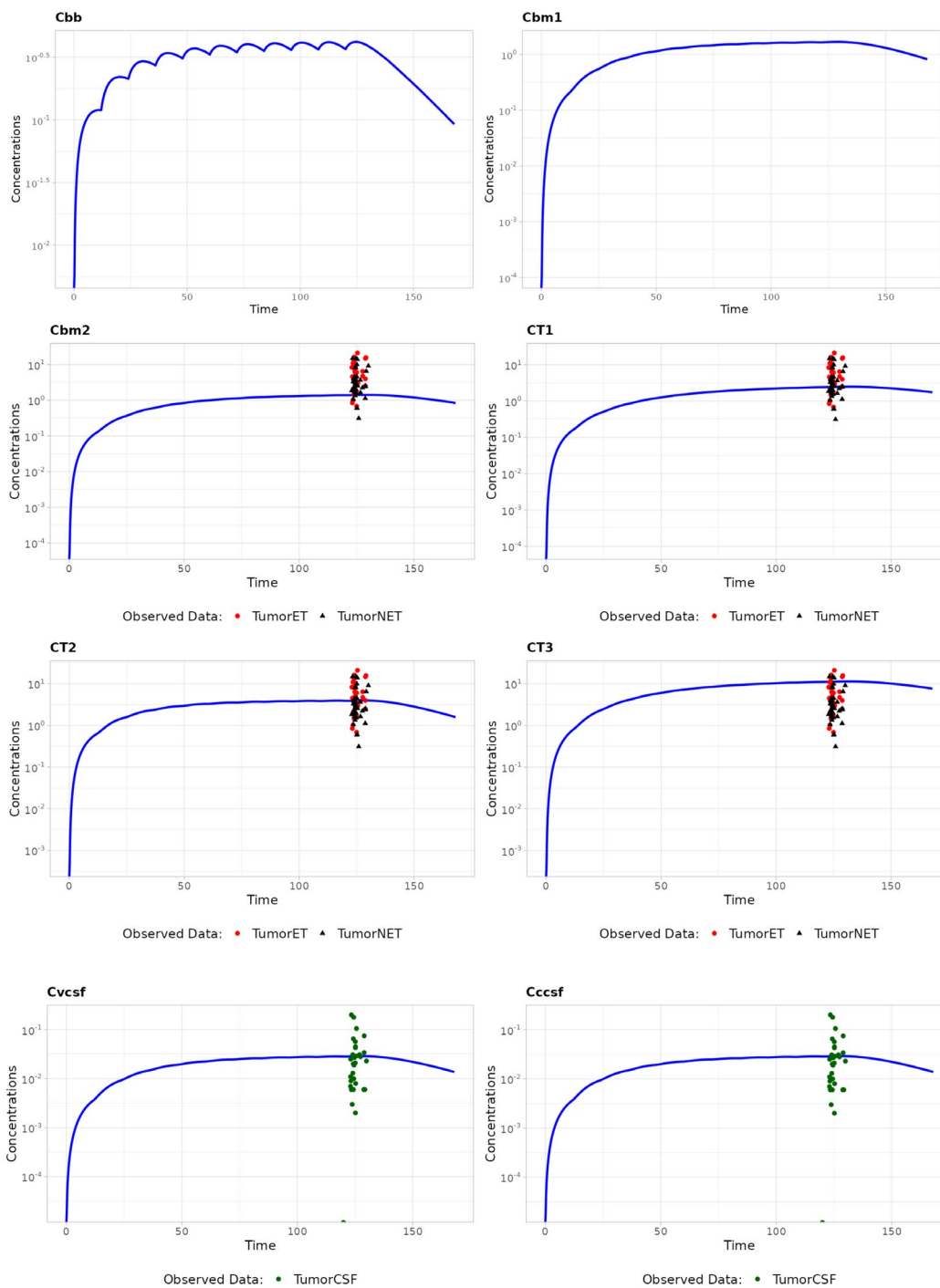


FIGURE 2 | Legend on next page.

**FIGURE 2** | A screenshot showing the simulated mean concentration-time profiles (in common logarithmic scale) of total abemaciclib in individual compartments of the 9-CNS model. The input file is provided in Table S2. The observed abemaciclib concentrations in the contrast-enhancing (shown in red symbols) and non-enhancing tumors (shown in black symbols) of glioblastoma patients are overlaid with the simulated mean total drug concentration-time profiles in the deep brain parenchyma compartment (Cbm2) and three tumor compartments including tumor rim (CT1), bulk tumor (CT2), and tumor core (CT3); the observed abemaciclib concentrations in CSF (shown in green symbols) are overlaid with the simulated mean total drug concentration-time profiles in three CSF compartments including ventricular CSF (Cvcfs), cranial subarachnoid CSF (Cccsf), and spinal subarachnoid CSF (Cscsf, not shown here due to the space limit).

of abemaciclib in the contrast-enhancing and non-enhancing tumors of glioblastoma patients are overlaid with the simulated mean total drug concentration—time profiles (in common logarithmic scale) for the deep brain parenchyma compartment (Cbm2) and three tumor compartments including tumor rim (CT1), bulk tumor (CT2), and tumor core (CT3); the observed total drug concentrations in CSF are overlaid with the simulated mean total drug concentration—time profiles for three CSF compartments including ventricular CSF (Cvcfs), cranial subarachnoid CSF (Cccsf), and spinal subarachnoid CSF (Cscsf).

The PK parameters (i.e.,  $C_{max}$ ,  $T_{max}$ , and AUC) for total or unbound drug can be estimated based on the simulated mean total/unbound drug concentration—time profiles in individual CNS compartments. Users have the flexibility to define the time interval for PK parameter calculation. By clicking “Pharmacokinetic parameters (total/unbound)” tab, users can view or download the PK parameter tables for both total and unbound drug.

#### 4.2.3 | View and Download Simulated Individual Concentration-Time Profiles and Inter-Individual Variability

The SpatialCNS-PBPK app has the capability of generating a patient population based on the mean values and interindividual variabilities (IIVs) of system- and drug-specific parameters that are provided in the input file. For example, if users want to generate a virtual population of  $n$  patients, the values of a particular system- or drug-specific parameter for these  $n$  patients are generated using Equation 1, where  $P$  is the mean parameter value provided in the input file, IIV is the interindividual variability for parameter  $P$ ,  $P_{vec}$  is a vector of size  $n$  with list of IIV based parameter values, and Norm generates random numbers from a standard normal distribution.

$$P_{vec} = e^{\left(\log\left(\frac{P}{\sqrt{1+IIV^2}}\right) + \left(\sqrt{\log(1+IIV^2)}\right)(x_i)\right)}; x_i \sim Norm(0, 1), i = 1, \dots, n \quad (1)$$

As an example, Table S3 shows the parameter values of system- and drug-specific parameters for five individual patients, generated by the app based on the mean parameter values (Sim1) and respective interindividual variability (IIV1) provided in the input file (Table S2). Users have the flexibility of defining the group size (i.e., number of patients) for a virtual population and perform simulations for individual patients. Users

can click “View simulated individual concentration-time profile” tab to view the simulated concentration data tables and profile plots (in either normal scale or normal logarithmic scale) for the total drug; in addition, users can download data tables as .csv files and plots as .pdf files. Figure 3 illustrates the simulated total drug concentration-time profiles of abemaciclib (in normal logarithmic scale) in individual CNS compartments for five individual patients. In addition, users can click “percentile plots” to view the mean, 5th and 95th percentiles of the simulated total drug concentration-time profiles (in normal scale or normal logarithmic scale) for a virtual population (Figure 4). Of note, if observed data are provided in the input file, observed data will be overlaid with the simulated percentile profiles, thus allowing visualization of the distribution of both observed and simulated concentration profiles. As illustrated in Figure 4, observed total abemaciclib concentrations in the contrast-enhancing and non-enhancing tumors of glioblastoma patients are overlaid with the simulated percentile profiles (50th, 5th, and 95th) of total drug concentrations for the deep brain parenchyma compartment (Cbm2) and three tumor compartments (i.e., tumor rim CT1, bulk tumor CT2, and tumor core CT3); the observed abemaciclib concentrations in CSF are overlaid with the simulated percentile profiles (50th, 5th, and 95th) of drug concentration in the three CSF compartments.

#### 4.3 | Perform Sensitivity Analysis

SpatialCNS-PBPK app provides sensitivity analysis function to examine the impact of a particular system- or drug-specific parameter on the concentration-time profiles in individual compartments of the 9-CNS model. This function is useful for parameter optimization to improve the model's predictivity. For example, to enable sensitivity analysis of a drug-specific parameter (e.g., PSB2, passive permeability clearance at the BBB between the blood and deep brain parenchyma compartments), users need to upload the input file (Table S2) and select the inputs for the sampling time (e.g., Time1), plasma concentration (e.g., Plasma1), and model parameter (e.g., Sim1); then, select the parameter name (e.g., PSB2), value range (e.g., from 2.5 to 250 L/h), and number of points (e.g., 5), and submit for sensitivity analysis (Figure 1). Of note, users can set the space between parameter points based on the uniform or normal logarithm of the parameter values. For example, when “uniform” is selected for parameter space, drug concentration-time profiles are simulated using the PSB values of 2.5, 64.4, 126.2, 188.1, and 250 L/h. When “log” is selected for parameter space, drug concentration-time profiles are simulated using the PSB values of 2.5, 7.9, 25, 79, and 250 L/h (Figure 5).

## Results: Mean and individual profiles

[View simulated mean concentration – time profiles](#)

[View simulated individual concentration – time profiles](#)

[Download simulated mean concentration – time profiles](#)

[Download simulated individual concentration – time profiles](#)

[Generated parameter list for given IIV](#)

[Concentration table](#)

[Concentration plots](#)

[Concentration log plots](#)

[Percentile data table](#)

[Percentile plots](#)

[Percentile log plots](#)

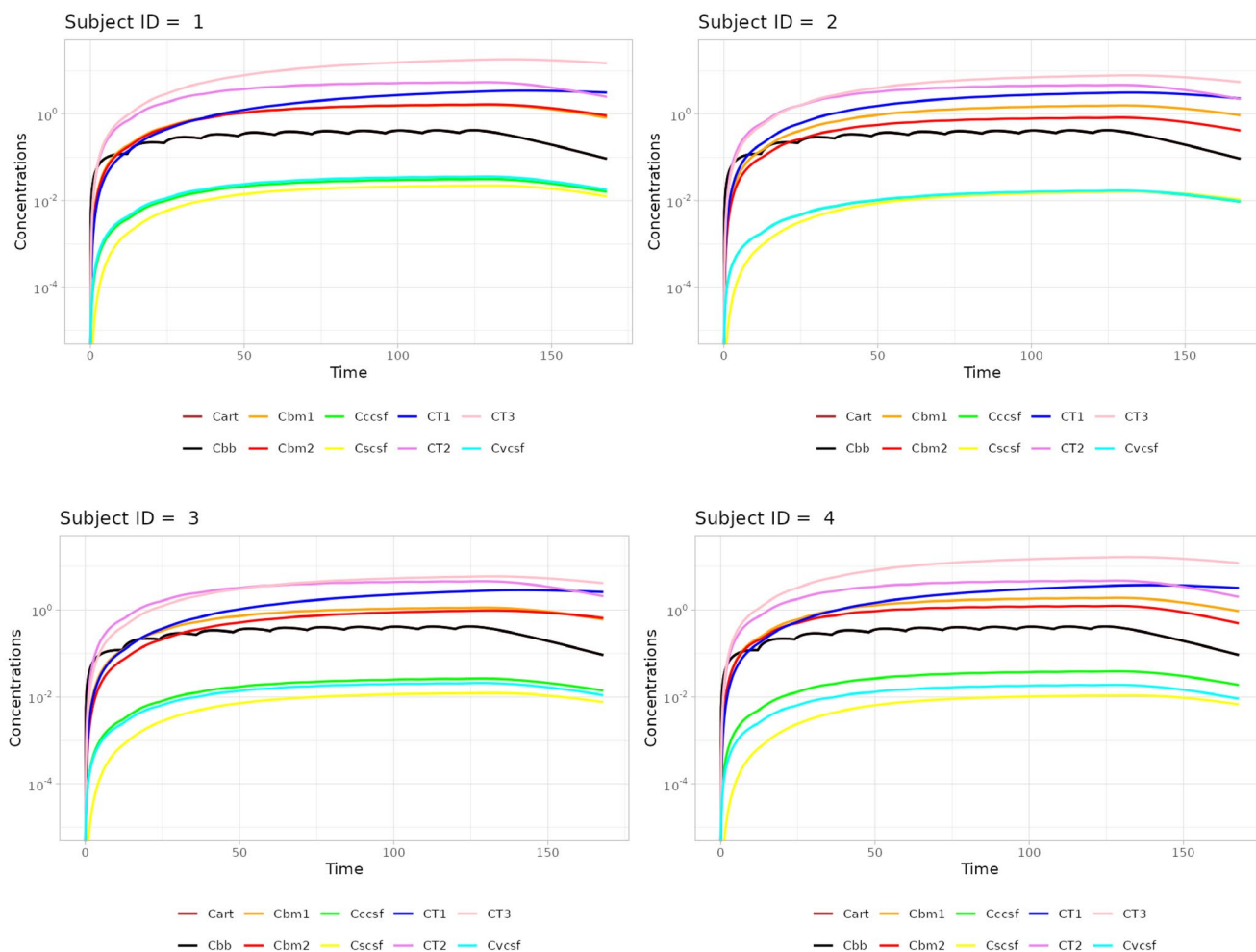


**FIGURE 3** | A screenshot showing the simulated concentration-time profiles (in common logarithmic scale) of total abemaciclib in the nine CNS compartments for individuals. The system- and drug-specific parameters for five individuals (shown in Table S3) were generated by the app based on the mean parameter values (Sim1) and respective IIVs (IIV1) provided in the input file (Table S2).

After sensitivity analysis is submitted, users can click “View parameter sensitivity simulation results” or “Download parameter sensitivity simulation results” tab to view or download the simulated concentration data tables and profile plots (in either normal scale or normal logarithmic scale) for total or unbound drug, as well as the calculated PK parameters (i.e.,  $T_{max}$ ,  $C_{max}$ , and AUC) and AUC scatter plot (i.e., the plot of AUC versus tested parameter values). For example, for sensitivity analysis of

PSB2 ranging from 2.5 to 250 L/h (at 5 parameter points using log space), Figure 5 illustrates the total drug concentration-time profiles in individual compartments simulated with the PSB2 values of 2.5, 7.9, 25, 79, and 250 L/h while other parameters remain the same as defined in the input “Sim1”. These data suggest that PSB2 significantly influences abemaciclib pharmacokinetic profile in the deep brain parenchyma compartment, while having negligible impacts on the PK profiles in other compartments.

# Results: Mean and individual profiles

[View simulated mean concentration – time profiles](#)

[View simulated individual concentration – time profiles](#)

[Download simulated mean concentration – time profiles](#)

[Download simulated individual concentration – time profiles](#)

[Generated parameter list for given IIV](#)

[Concentration table](#)

[Concentration plots](#)

[Concentration log plots](#)

[Percentile data table](#)

[Percentile plots](#)

**[Percentile log plots](#)**

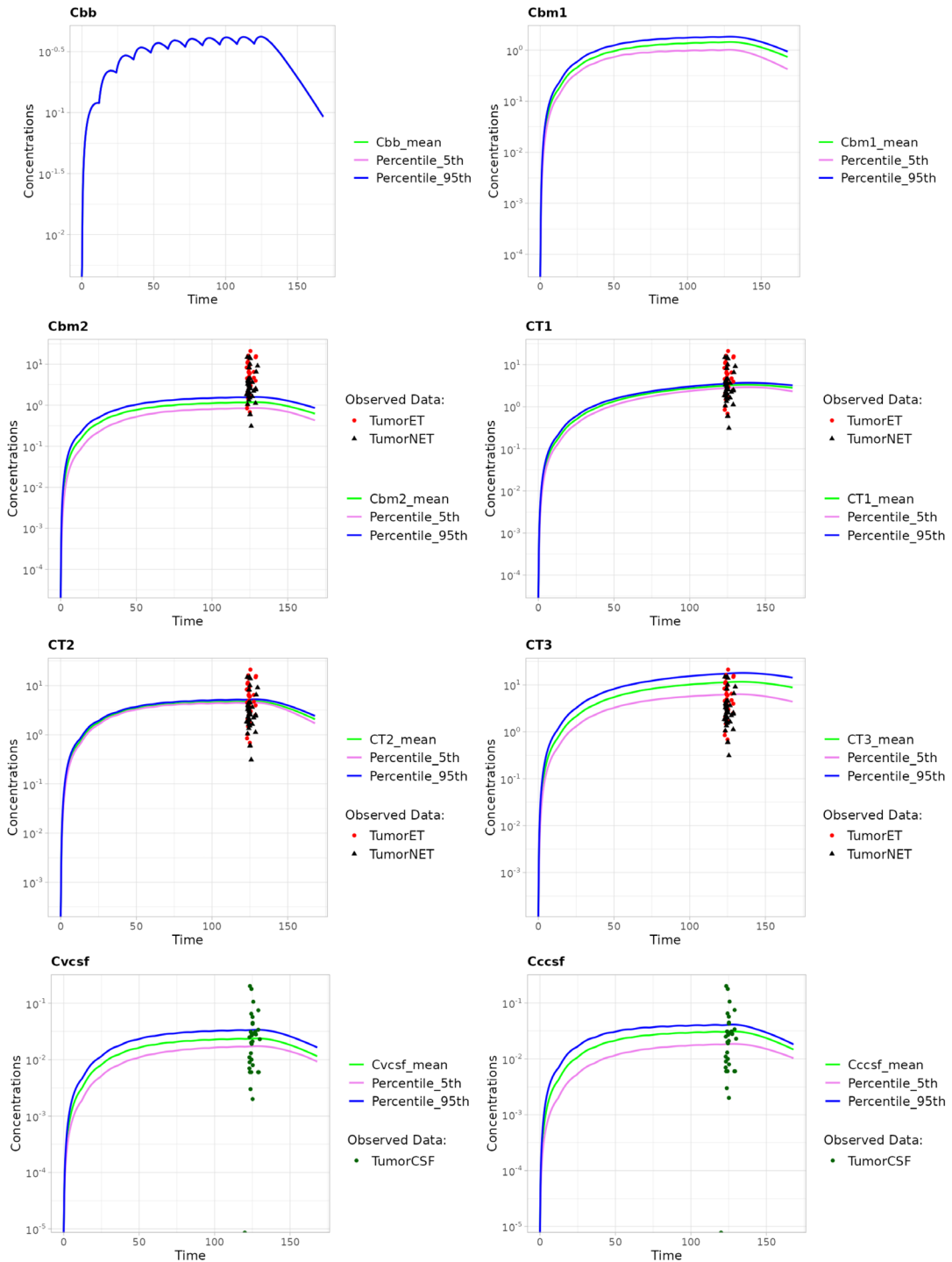


**FIGURE 4** | A screenshot showing the simulated mean, 5th and 95th percentiles of the concentration-time profiles (in common logarithmic scale) of total abemaciclib in individual compartments of the 9-CNS model from five individuals. The input file is provided in Table S2. The observed abemaciclib concentrations in the contrast-enhancing (shown in red symbols) and non-enhancing tumors (shown in black symbols) of glioblastoma patients are overlaid with the simulated percentile concentration-time profiles in the deep brain parenchyma compartment (Cbm2) and three tumor compartments including tumor rim (CT1), bulk tumor (CT2), and tumor core (CT3); the observed abemaciclib concentrations in CSF (shown in green symbols) are overlaid with the simulated percentile concentration-time profiles in three CSF compartments including ventricular CSF (Cvcfs), cranial subarachnoid CSF (Cccsf), and spinal subarachnoid CSF (Cscsf, not shown here due to the space limit).

Based on the simulated concentration-time profiles, the SpatialCNS-PBPK app is capable of calculating PK parameters (i.e.,  $T_{max}$ ,  $C_{max}$ , and AUC) for any user-defined time interval (e.g., 72–96 h). Users can view or download PK parameter tables for total and unbound drug. In addition, users can view or download the AUC scatter plots, which provide a direct visualization of the impact of the tested parameter (e.g., PSB2) on drug exposure (AUC) in individual CNS compartments. As illustrated in Figure 6, PSB2 has a significant impact on the total drug exposure (AUC) of abemaciclib in the deep brain parenchyma, but not in the other CNS compartments.

## 5 | Discussion

In our previous study, we developed and rigorously validated an innovative mechanism-based 9-CNS PBPK model for the quantitative prediction of spatial pharmacokinetics of systemically administered drugs in the human CNS and brain tumors [7]. In the present study, we developed the SpatialCNS-PBPK app, a user-friendly, web-based platform designed to make the 9-CNS model accessible to a broad range of researchers, scientists, and drug developers. The app includes key functionalities such as model simulation, sensitivity analysis, and pharmacokinetic parameter calculation. To ensure reliability, we validated the methodology and simulation function of the app by comparing its outputs with those from a standard PBPK modeling & simulation software (Simcyp Simulator). This tutorial provides a step-by-step user guide for practical applications and also explains the pharmacological and mathematical basis underlying the platform's development. This ensures that users gain a comprehensive understanding of the SpatialCNS-PBPK app's functionality, rather than treating it as a “black box”. Important, while the app is built on advanced computation modeling, it is designed to be intuitive and does not require users to have advanced statistical or programming expertise.

One of the challenges in developing and applying the 9-CNS PBPK model lies in the uncertainties surrounding some system-specific parameters, particularly those related to tumor compartments. Critical parameters such as efflux/uptake transporter protein abundances at the BBTB, degree of BBTB disruption, tumor weight, tumor vasculature surface area, and regional pH are not readily available and are difficult—if not impossible—to quantify in patients, even with advanced imaging technologies. Moreover, these parameters exhibit significant intra- and inter-individual variability, further complicating model development. A major advantage of our approach was access to rich clinical plasma and CNS pharmacokinetic data for six drugs [7]. These data included total and unbound drug concentrations in the

plasma, paired contrast-enhancing and non-enhancing tumor regions, and CSF, which provided a robust foundation for defining tumor-specific parameters in a stepwise, iterative manner. Specifically, during initial model development, we assigned tumor-specific parameters based on prior knowledge and literature data. In the model optimization phase, we refined these parameters through a series of simulations, comparing simulated drug concentration profiles with observed clinical data. This learn-confirm-refine iterative process allowed us to rigorously define and validate system-specific parameters using six drugs [7]. The final validated system-specific parameters (as presented in Tables 1 and 2 and the input file template) serve as default starting values for users. However, the SpatialCNS-PBPK app offers flexibility, allowing users to modify both system-specific and drug-specific parameters to better fit their specific drugs and applications.

The 9-CNS PBPK model offers a unique advantage by enabling the prediction of spatiotemporal drug penetration and exposure in the human CNS and brain tumors based on plasma concentration–time profiles, irrespective of the route of systemic drug administration. Since drug plasma concentrations can be readily measured in individual patients or a population, this model serves as a powerful computational tool for prospectively and reliably predicting spatial pharmacokinetics in the human CNS and brain tumors across various clinical settings and patient populations. The quantitative insights gained from this model are invaluable for guiding efficient clinical trial designs, selecting optimal drug candidates, and refining dosing regimens. Notably, a significant challenge in treating brain tumors is the substantial inter-individual variability and spatial heterogeneity in drug penetration and exposure, making one-size-fits-all treatment strategies often ineffective. The 9-CNS PBPK model addresses this challenge by enabling individualized dosing regimens. By leveraging observed plasma concentration–time profiles and patient-specific brain or tumor characteristics, the model can predict drug exposure in the CNS and tumors in an individual patient. If the predicted drug exposure is suboptimal, alternative dosing regimens can be simulated to determine the optimal strategy for achieving therapeutic drug concentrations in the brain and tumor tissue.

In summary, the SpatialCNS-PBPK app enhances our ability to predict the spatial pharmacokinetics of anticancer drugs in the human CNS and brain tumors with greater accuracy and efficiency. This invaluable computational tool supports the development of more effective therapies and the optimized use of existing drugs, ultimately improving treatment outcomes for brain cancer patients.

## Results: Sensitivity analysis

View parameter sensitivity simulation results

Download parameter sensitivity simulation results

Concentration table(Total)

Concentration plots(Total)

Concentration log plots(Total)

PK parameters(Cmax, Tmax, AUC)(Total)

AUC scatter plots(Total)

Concentration table(Unbound)

Concentration plots(Unbound)

Concentration log plots(Unbound)

PK parameters(Cmax, Tmax, AUC)(Unbound)

AUC scatter plots(Unbound)

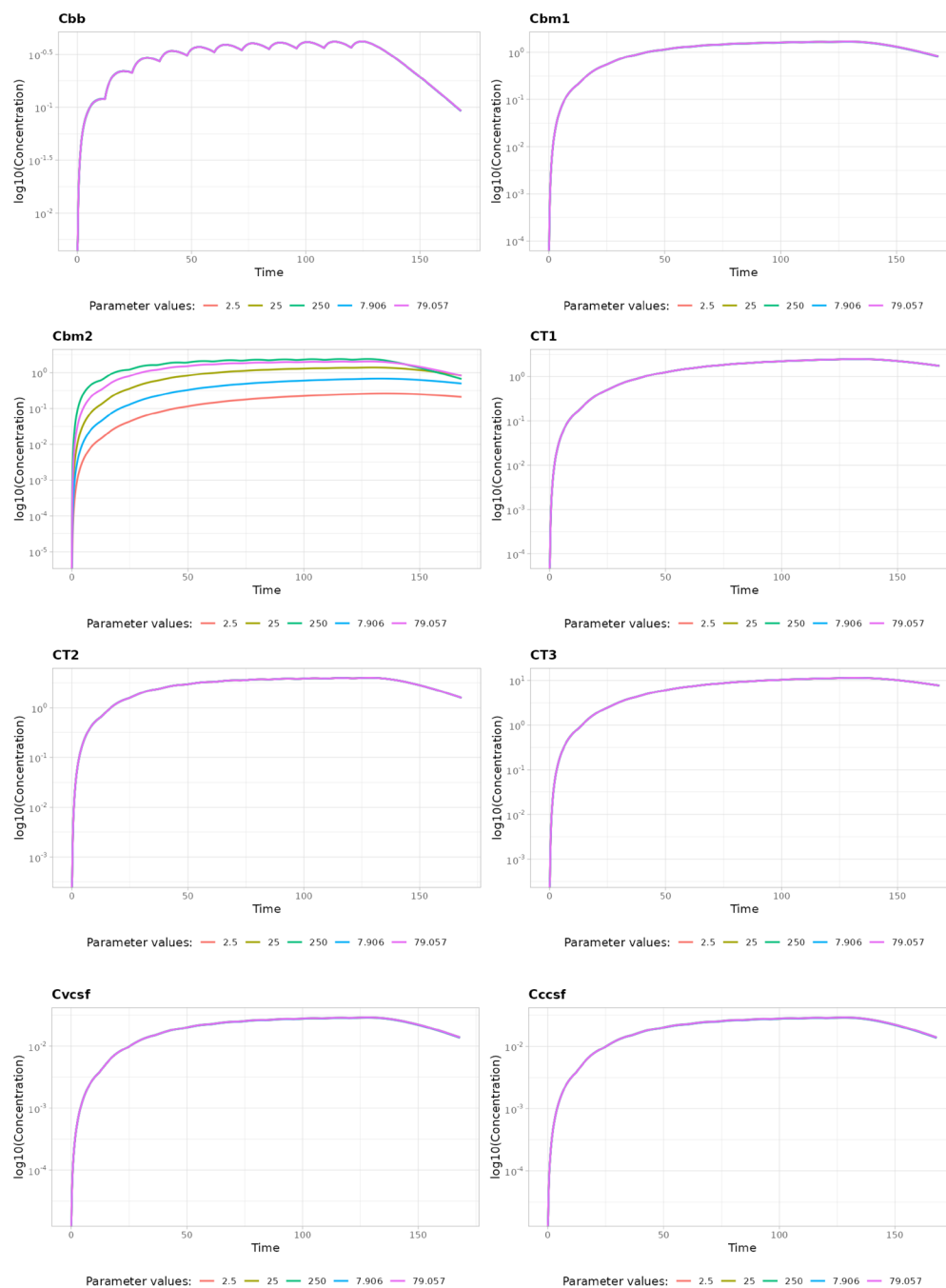


**FIGURE 5** | A screenshot showing the sensitivity analysis of the impact of PSB2 (passive permeability clearance at the BBB between the blood and deep brain parenchyma compartments) on the total abemaciclib concentration—time profiles in individual CNS compartments. Sensitivity analysis was performed with the PSB2 values of 2.5, 7.9, 25, 79, and 250L/h while other parameters remain the same as provided in the input “Sim1” (Table S2).

## Results: Sensitivity analysis

View parameter sensitivity simulation results

Download parameter sensitivity simulation results

Concentration table(Total)

Concentration plots(Total)

Concentration log plots(Total)

PK parameters(Cmax, Tmax, AUC)(Total)

AUC scatter plots(Total)

Concentration table(Unbound)

Concentration plots(Unbound)

Concentration log plots(Unbound)

PK parameters(Cmax, Tmax, AUC)(Unbound)

AUC scatter plots(Unbound)

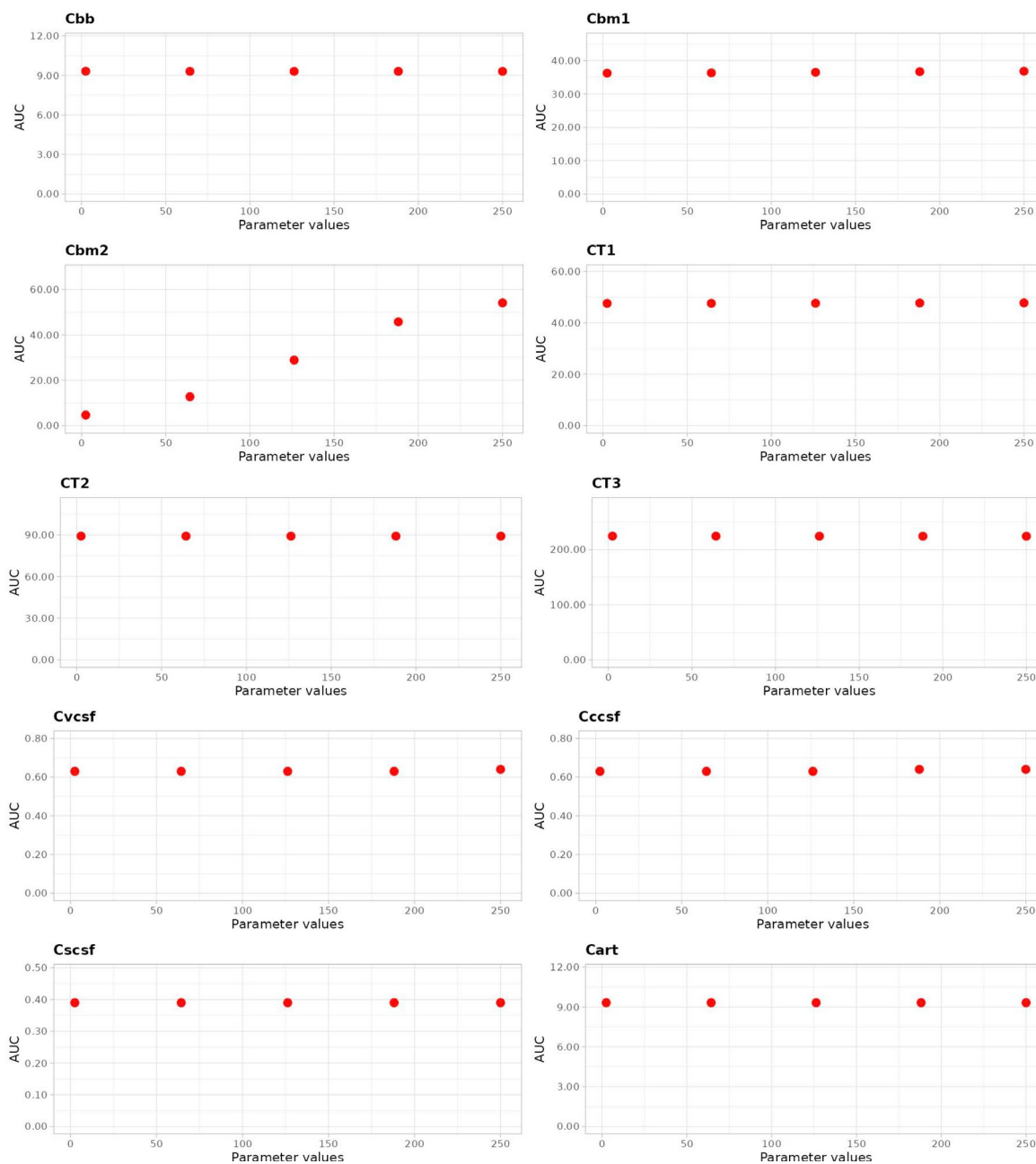


**FIGURE 6** | A screenshot showing the sensitivity analysis of the impact of PSB2 (passive permeability clearance at the BBB between the blood and deep brain parenchyma compartments) on the total abemaciclib drug exposure (i.e., AUC) in individual CNS compartments. Sensitivity analysis was performed with the PSB2 values of 2.5, 7.9, 25, 79, and 250 L/h while other parameters remain the same as provided in the input “Sim1” (Table S2).

---

## Conflicts of Interest

The authors declare no conflicts of interest.

## Data Availability Statement

The data used to perform simulations in this study are available within the paper and [Supporting Information](#). A patent application (US 63/684,242) for the 9-CNS PBPK model platform is currently under review. Once the patent is granted, the R/Shiny codes for the model will be available from the corresponding author upon reasonable request.

## References

1. A. Bhowmik, R. Khan, and M. K. Ghosh, "Blood Brain Barrier: A Challenge for Effectual Therapy of Brain Tumors," *BioMed Research International* 2015 (2015): 320941.
2. S. Watkins, S. Robel, I. F. Kimbrough, S. M. Robert, G. Ellis-Davies, and H. Sontheimer, "Disruption of Astrocyte-Vascular Coupling and the Blood-Brain Barrier by Invading Glioma Cells," *Nature Communications* 5 (2014): 4196.
3. P. R. Lockman, R. K. Mittapalli, K. S. Taskar, et al., "Heterogeneous Blood-Tumor Barrier Permeability Determines Drug Efficacy in Experimental Brain Metastases of Breast Cancer," *Clinical Cancer Research* 16 (2010): 5664–5678.
4. E. R. Gerstner and R. L. Fine, "Increased Permeability of the Blood-Brain Barrier to Chemotherapy in Metastatic Brain Tumors: Establishing a Treatment Paradigm," *Journal of Clinical Oncology* 25 (2007): 2306–2312.
5. P. Zhao, L. Zhang, J. A. Grillo, et al., "Applications of Physiologically Based Pharmacokinetic (PBPK) Modeling and Simulation During Regulatory Review," *Clinical Pharmacology & Therapeutics* 89 (2011): 259–267.
6. P. Poulin and F.-P. Theil, "Prediction of Pharmacokinetics Prior to In Vivo Studies. II. Generic Physiologically Based Pharmacokinetic Models of Drug Disposition," *Journal of Pharmaceutical Sciences* 91 (2002): 1358–1370.
7. J. Li, C. Wickramasinghe, J. Jiang, et al., "Mechanistic Modeling of Spatial Heterogeneity of Drug Penetration and Exposure in the Human Central Nervous System and Brain Tumors," *Clinical Pharmacology and Therapeutics* 117 (2024): 690–703.
8. M. Jamei, S. Marciniak, K. Feng, A. Barnett, G. Tucker, and A. Rostami-Hodjegan, "The Simcyp® Population Based ADME Simulator," *Expert Opinion on Drug Metabolism & Toxicology* 5 (2009): 211–223.
9. P. Vaddady and B. Kandala, "ModVizPop: A Shiny Interface for Empowering Teams to Perform Interactive Pharmacokinetic/Pharmacodynamic Simulations," *CPT: Pharmacometrics & Systems Pharmacology* 10 (2021): 1323–1331.
10. J. Wojciechowski, A. M. Hopkins, and R. N. Upton, "Interactive Pharmacometric Applications Using R and the Shiny Package," *CPT: Pharmacometrics & Systems Pharmacology* 4 (2015): e00021.
11. H. Cho and E. K. Lee, "PKconverter: R Package to Convert the Pharmacokinetic Parameters," *Translational and Clinical Pharmacology* 27 (2019): 73–79.
12. T. Lu, V. Poon, L. Brooks, et al., "gPKPDviz: A Flexible R Shiny Tool for Pharmacokinetic/Pharmacodynamic Simulations Using Mrgsolve," *CPT: Pharmacometrics & Systems Pharmacology* 13 (2024): 341–358.
13. W. Chang, J. Cheng, J. J. Allaire, et al., "shiny: Web Application Framework for R. R Package Version 1.6. 0," 2021, <https://CRAN.R-project.org/package=shiny>.
14. H. Wickham, M. Averick, J. Bryan, et al., "Welcome to the Tidyverse," *Journal of Open Source Software* 4 (2019): 1686.
15. K. Soetaert, T. Petzoldt, and R. W. Setzer, "Solving Differential Equations in R: Package deSolve," *Journal of Statistical Software* 33, no. 9 (2010): 1–25, <https://doi.org/10.18637/jss.v033.i09>.
16. H. Wickham and H. Wickham, "Getting Started With ggplot2," in *ggplot2: Elegant Graphics for Data Analysis* (Springer Cham, 2016), 11–31.
17. H. Wickham, R. Francois, L. Henry, and K. Müller, "dplyr. A Grammar of Data Manipulation," 2020.
18. L. Gaohua, S. Neuhoff, T. N. Johnson, A. Rostami-Hodjegan, and M. Jamei, "Development of a Permeability-Limited Model of the Human Brain and Cerebrospinal Fluid (CSF) to Integrate Known Physiological and Biological Knowledge: Estimating Time Varying CSF Drug Concentrations and Their Variability Using In Vitro Data," *Drug Metabolism and Pharmacokinetics* 31 (2016): 224–233.
19. J. Li, J. Jiang, X. Bao, et al., "Mechanistic Modeling of Central Nervous System Pharmacokinetics and Target Engagement of HER2 Tyrosine Kinase Inhibitors to Inform Treatment of Breast Cancer Brain Metastases," *Clinical Cancer Research* 28 (2022): 3329–3341.
20. J. Li, J. Jiang, J. Wu, X. Bao, and N. Sanai, "Physiologically Based Pharmacokinetic Modeling of Central Nervous System Pharmacokinetics of CDK4/6 Inhibitors to Guide Selection of Drug and Dosing Regimen for Brain Cancer Treatment," *Clinical Pharmacology and Therapeutics* 109 (2021): 494–506.
21. S. B. Hladky and M. A. Barrand, "Mechanisms of Fluid Movement Into, Through and out of the Brain: Evaluation of the Evidence," *Fluids and Barriers of the CNS* 11 (2014): 26.
22. L. Sakka, G. Coll, and J. Chazal, "Anatomy and Physiology of Cerebrospinal Fluid," *European Annals of Otorhinolaryngology, Head and Neck Diseases* 128 (2011): 309–316.
23. J. Li, A. Wu, and S. Kim, "Mechanistic Modeling of Intrathecal Chemotherapy Pharmacokinetics in the Human Central Nervous System," *Clinical Cancer Research* 30 (2024): 1397–1408.
24. J. J. Iliff, M. Wang, Y. Liao, et al., "A Paravascular Pathway Facilitates CSF Flow Through the Brain Parenchyma and the Clearance of Interstitial Solutes, Including Amyloid Beta," *Science Translational Medicine* 4 (2012): 147ra111.
25. X. Bao, J. Wu, Y. Xie, et al., "Protein Expression and Functional Relevance of Efflux and Uptake Drug Transporters at the Blood-Brain Barrier of Human Brain and Glioblastoma," *Clinical Pharmacology and Therapeutics* 107 (2020): 1116–1127.
26. A. Honasoge and H. Sontheimer, "Involvement of Tumor Acidification in Brain Cancer Pathophysiology," *Frontiers in Physiology* 4 (2013): 316, <https://doi.org/10.3389/fphys.2013.00316>.
27. X. Zhang, Y. Lin, and R. J. Gillies, "Tumor pH and Its Measurement," *Journal of Nuclear Medicine* 51 (2010): 1167–1170.
28. J. R. Casey, S. Grinstein, and J. Orłowski, "Sensors and Regulators of Intracellular pH," *Nature Reviews. Molecular Cell Biology* 11 (2010): 50–61.
29. A. C. Hindmarsh and L. R. Petzold, "LSODA, Ordinary Differential Equation Solver for Stiff or Non-Stiff System," 2005.
30. J. D. Lambert, *Computational Methods in Ordinary Differential Equations* (Wiley, 1973).
31. C. W. Gear, *Numerical Initial Value Problems in Ordinary Differential Equations*, Prentice-Hall series in automatic computation. (Prentice Hall, 1971).
32. L. Shampine, "Stiffness and the Automatic Selection of ODE Codes," *Journal of Computational Physics* 54 (1984): 74–86.

33. K. Radhakrishnan and A. C. Hindmarsh, "Description and Use of LSODE, the Livermore Solver for Ordinary Differential Equations," 1993.
34. K. P. Cosgrove, C. M. Mazure, and J. K. Staley, "Evolving Knowledge of Sex Differences in Brain Structure, Function, and Chemistry," *Biological Psychiatry* 62 (2007): 847–855.
35. C. S. Sinnatamby, *Last's Anatomy* (Churchill Livingstone/Elsevier, 2011).
36. H. F. Cserr, D. N. Cooper, P. K. Suri, and C. S. Patlak, "Efflux of Radiolabeled Polyethylene Glycols and Albumin From Rat Brain," *American Journal of Physiology* 240 (1981): F319–F328.
37. M. Edsbacke, M. Tisell, L. Jacobsson, and C. Wikkelso, "Spinal CSF Absorption in Healthy Individuals," *American Journal of Physiology. Regulatory, Integrative and Comparative Physiology* 287 (2004): R1450–R1455.
38. J. Li, J. Jiang, J. Wu, X. Bao, and N. Sanai, "Physiologically Based Pharmacokinetic Modeling of Central Nervous System Pharmacokinetics of CDK4/6 Inhibitors to Guide Selection of Drug and Dosing Regimen for Brain Cancer Treatment," *Clinical Pharmacology and Therapeutics* 109 (2020): 494–506.
39. A. C. Tien, J. Li, X. Bao, et al., "A Phase 0 Trial of Ribociclib in Recurrent Glioblastoma Patients Incorporating a Tumor Pharmacodynamic- and Pharmacokinetic-Guided Expansion Cohort," *Clinical Cancer Research* 25 (2019): 5777–5786.
40. S. Mehta, R. Fiorelli, X. Bao, et al., "A Phase 0 Trial of Ceritinib in Patients With Brain Metastases and Recurrent Glioblastoma," *Clinical Cancer Research* 28 (2022): 289–297.
41. N. C. Y. Sanai, T. Margaryan, A. DeSantis, et al., "A Phase 0 'Trigger' Trial of CDK4/6 Plus ERK1/2 Inhibitors in Recurrent Glioblastoma," *Journal of Clinical Oncology* 39, no. 15\_suppl (2021): 2005, [https://doi.org/10.1200/JCO.2021.39.15\\_suppl.2005](https://doi.org/10.1200/JCO.2021.39.15_suppl.2005).
42. T. Margaryan, M. Elliott, N. Sanai, and A. Tovmasyan, "Simultaneous Determination of LY3214996, Abemaciclib, and M2 and M20 Metabolites in Human Plasma, Cerebrospinal Fluid, and Brain Tumor by LC-MS/MS," *Journal of Pharmaceutical Analysis* 12 (2022): 601–609.
43. W. R. Kennedy, Y. W. Chang, J. Jiang, et al., "A Combined Phase 0/2 'Trigger' Trial Evaluating Pamiparib or Olaparib With Concurrent Radiotherapy in Patients With Newly-Diagnosed or Recurrent Glioblastoma," *International Journal of Radiation Oncology, Biology, Physics* 117 (2023): e115.
44. K. T. A. Johnson, J. Jiang, J. McNamara, et al., "Single Cell Transcriptomics, Pharmacokinetics, and Pharmacodynamics of Combined CDK4/6 and MTOR Inhibition in a Phase 0 Trial of Recurrent High-Grade Glioma," *Neuro-Oncology* 25 (2023): v78–v79.
45. X. Bao, J. Wu, N. Sanai, and J. Li, "A Liquid Chromatography With Tandem Mass Spectrometry Method for Quantitating Total and Unbound Ceritinib in Patient Plasma and Brain Tumor," *Journal of Pharmaceutical Analysis* 8 (2018): 20–26.
46. X. Bao, J. Wu, N. Sanai, and J. Li, "Determination of Total and Unbound Ribociclib in Human Plasma and Brain Tumor Tissues Using Liquid Chromatography Coupled With Tandem Mass Spectrometry," *Journal of Pharmaceutical and Biomedical Analysis* 166 (2019): 197–204.

### Supporting Information

Additional supporting information can be found online in the Supporting Information section.